Spatial and Geological Distribution of Mars Craters from MOLA Data

Marin Vojković

Supervisor: dr. Dejan Vinković

Split, October 2012

Master Thesis in Physics

Department of Physics
Faculty of Natural Sciences and Mathematics
University of Split

Abstract

The new Martian crater catalogue MA132843GT provides us with the opportunity to study the statistical properties of Martian craters on a planetary scale. We identify the crater depth d and diameter D as main parameters to describe crater morphology and determine their relationship as a broken power law $d = 0.14 \cdot D^{1.28}$ for simple craters and $d = 0.66 \cdot D^{0.35}$ for complex craters. Using these data we created a catalogue of artificial pristine craters to compare it with real world data. Analysis shows that reduction of crater depth can be used as a parameter to approximate crater age. Various erosion processes reduce the crater depth, while leaving its diameter intact. Hence, a comparison of the measured crater d/D ratio with its pristine version can be used as a measure of its decay. When calculating crater number density and relative crater distribution on Martian surfaces of different age age we can notice that older surfaces have much fewer deep craters, but more eroded ones. In crater density analysis we compared the profiles of real craters with the profiles made from pristine catalogue to get a better estimate of how the surface profile changes with age. Grouping of surfaces by age is based on geological data obtained for Mars and is supported by crater count analysis. Spatial and geographical distributions show relative uniformity across Martian surface as would be expected, except that deep craters are located mostly within $\pm 50^{\circ}$ Mars latitude. This is most probably a signature of variable cryosphere depth or relatively more abundant number of impactors coming from the ecliptic.

Acknowledgements

I would like to acknowledge dr. Goran Salamunićcar for letting me use the new MA132843GT Martian impact craters catalogue, created by himself and dr. Sven Lončarić, and for his very important support throughout the work.

Contents

List of Figures

Chapter 1

Introduction

Impact craters are among the most abundant geological features in the Solar system. They are found in large numbers on every solid object - be it a planet, satellite, asteroid or a comet. Earth itself has gone through extensive bombardments throughout its history, but as our planet is geologically very active, many of the craters eroded and cannot be detected anymore. That makes Earth unsuitable for study of crater properties. Since the size of the impactor (and consequently the size of the blast and left-over crater) can vary trough several orders of magnitude, some impacts can have global consequences. Therefore, it is important to know and understand the mechanism behind this process.

When an impactor hits the ground, after passing through the atmosphere, the pressure on the impact site increases enormously. This phase is followed by the decompression phase. Decompression process is in fact very similar to a classical explosion. Due to the high pressure and temperature, the impactor is instantly disintegrated. Material from both the impactor and surface is ejected in cone-shaped pattern. Ejection of the material causes the transitional crater cavity to form. This cavity is bowl-shaped and has the geometry of a semi sphere. When the ejected material begins to fall back the cavity is partially filled by this debris. Also, the walls of the transitional cavity begin to collapse causing the characteristically flattened crater floor.

Cater formed by the impact can be simple or complex, depending on the size of the impactor. Simple craters have rounded walls, elevated crater rim and flattened floors. Complex craters also have elevated rims and rounded walls, but have either a central elevation on the crater floor or a elevated ring in the center of the floor. Very large impact craters can have several central ring formations. Complex craters are also shallower than simple craters and they are created from big impacts, while simple craters result from small impactors.

The theory of simple impact craters distinguishes between the strength regime and the gravity regime of cratering. The gravity regime is applicable when the soil strength is much smaller than the gravity pressure. The crater properties are then dictated by the impactors size and velocity and planet surface gravity. This happens for about kilometer-sized impactors. Strength regime is applicable for smaller impacts when the strength of the surface represents an important factor in the cratering process.

With the recent development of the new MA132843GT catalogue of Martian impact craters by Salamunicćar, Lončarić (2012), we now have a chance to study their statistical properties on a planetary scale. In this dissertation we will examine several statistical distributions of some important crater features. We will take a look at the spatial crater distribution across the whole surface, crater density profiles for different Martian surfaces and examine their link to surface age. We will also study the relationship of craters size (diameter) to its depth and its depth/diameter ratio. These are identified as the main morphological parameters for impact craters. For comparison and better understanding of erosion process, we created an artificial catalogue of pristine craters. This will serve as comparison with measured data to possibly distinguish the features of the crater distribution which are affected by erosion and crater age.

Chapter 2

MA132843GT catalogue

New possibilities for crater research on a global scale opened up with the new MA132843GT catalogue. It so far the most complete publicly available catalogue of Martian craters which distinguishes craters of up to D=2km (Salamuniccar, Lončarić, 2012). This catalogue is an extension of the previous MA130301GT catalogue which included 57,633 craters from previously manually assembled catalogues and 72,668 craters identified using several crater detection algorithms (CDAs) (Salamuniccar, Lončarić, 2012). The CDA developed by dr.Goran Salamunićcar and dr.Sven Lončarić uses fuzzy logic edge detection and Radon/Hough transform (Salamuniccar, Lončarić, 2010). It is designed to work with digital elevation models (DEM), in this case obtained from Mars Orbital Laser Altimeter (MOLA) mounted on Mars Global Surveyor (MGS). Figure 2.1 shows Mars surface from MOLA data. This CDA possesses high detection rate, with highly reduced number of false detections. Furthermore in the process of the catalogue creation all of the new detections were examined manually to filter out possible mistakes (Salamuniccar, Lončarić, 2010).

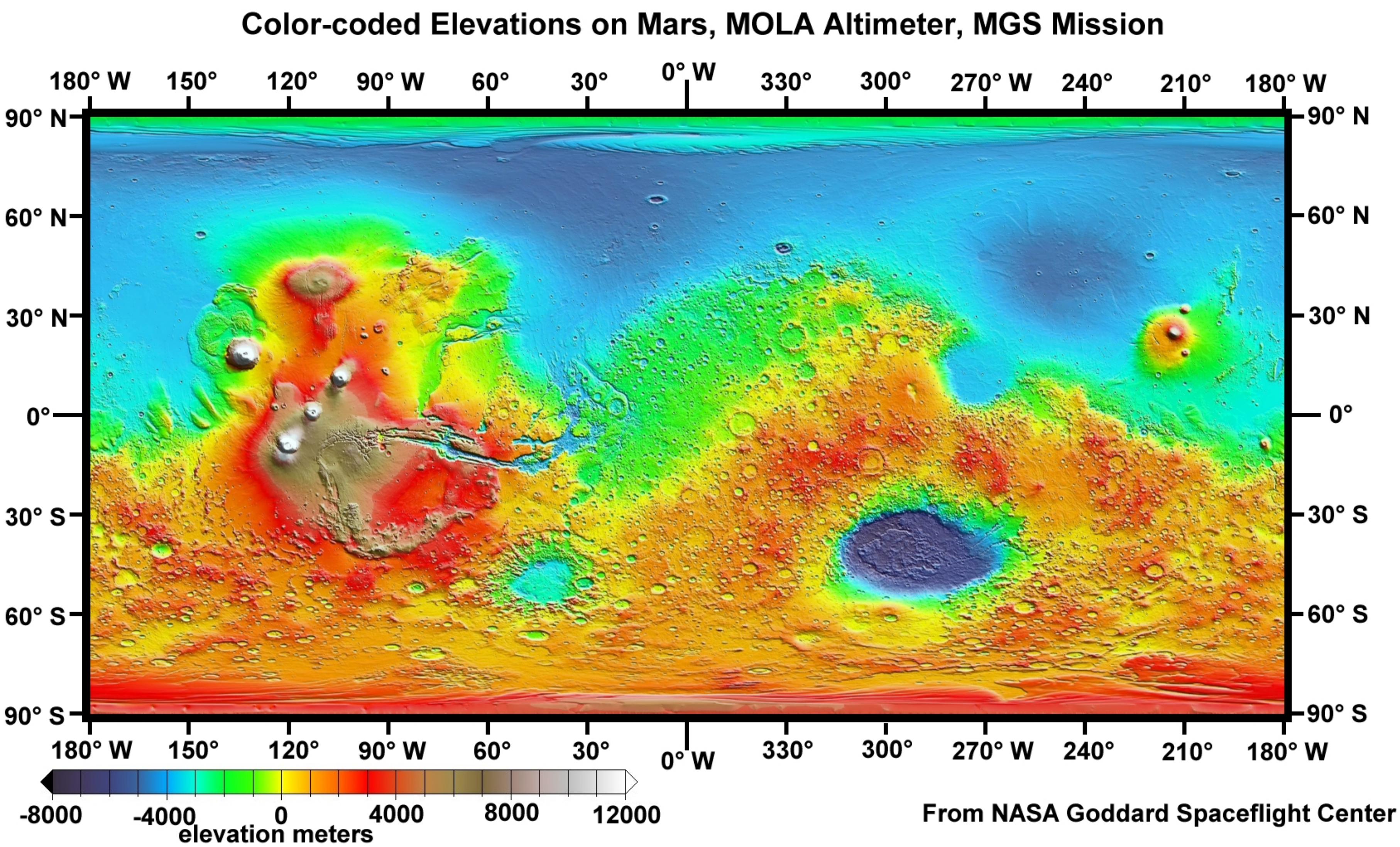

Figure 2.1: Representation of the surface of Mars from data obtained by MOLA (Mars Orbital Laser Altimeter). Ground elevation is shown with different coloring. (Treiman, 2003)

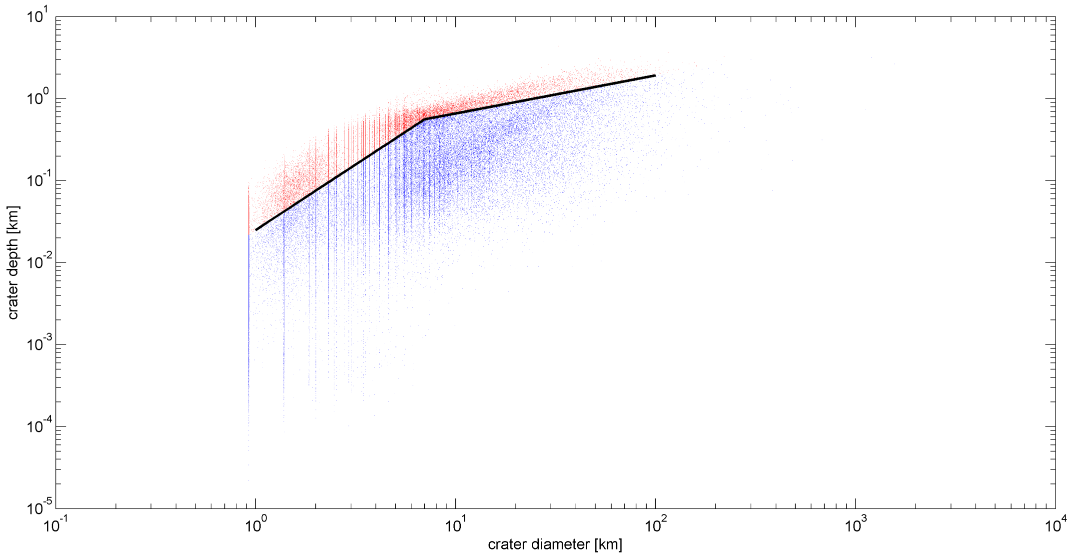

Figure 2.2: Depth against diameter on a log-log scale for MA132843GT craters (red - deep craters, blue - shallow craters). The deep craters are the ones above the line $d = 0.025 \cdot D^{1.6}$ for simple craters ($D < 7km$) and above $d = 0.22 \cdot D^{0.47}$ for complex craters ($D \geq 7km$). This kind of division is proposed by Stepinski et. al. (2009).

2.1 Crater depths and diameters

Crater depth d, diameter D and their ratio d/D are good parameters for describing crater shape in a large scale analysis of crater morphology. Crater depth is measured as distance between the highest and the lowest point of the crater. Diameter is measured at the top of the elevated rim. Because of the physics of the crater formation process, depth/diameter ratio follows a specific broken power law for freshly formed craters. As the crater gets older its depth decreases due to erosion processes and redeposition of material. We will examine this in more detail in section 2.2. The broken power law is different for simple ($D < 7km$) and complex ($D \geq 7km$) craters. Besides the simple/complex division, craters can be also characterized as deep or shallow based on their depth and diameter. Deep simple craters have $d \geq 0.025 \cdot D^{1.6}$, while deep complex crater have $d \geq 0.22 \cdot D^{0.47}$ (Stepinski et. al., 2009). Shallow craters are the ones with $d < 0.025 \cdot D^{1.6}$ for simple and $d < 0.22 \cdot D^{0.47}$ for complex craters. This division is shown in Figure 2.2.

Depth/diameter ratio against diameter distribution also reveals some interesting connections (Figure 2.3). As craters diameters span across three orders of magnitude it is convenient to plot them in log scale for diameter (y-axis), but for a comparison reference it is still useful to plot it in linear scale as well. As vast majority of craters have D¡30km we divided craters into 6 bins according to their diameter. These will be used in further analysis of the crater properties. In Figure 2.2 some vertical groupings (vertical lines) of the craters can be observed for craters with $D < 10km$. As MOLA's vertical roughness is measured at 100m scale (Smith et. al., 2001), smaller craters are represented with fewer data points, so their depth and (especially) diameter and profile have a considerable measuring error. This causes many of the craters that have similar but not the same diameter to appear to have identical diameter listed in the catalogue, thus causing vertical groupings. Since the size frequency distribution of the Martian craters is a smooth function not favoring any particular diameter (Ivanov, Neukum et.al., 2002) we can assume that this kind of grouping is indeed not a result of any natural process but has to do with data collection process.

All of the crater bins in Figure 2.3, except for the first one, show linear trends of depth/diameter decreasing with increasing diameter. For better view of the data distribution, top figure is the same

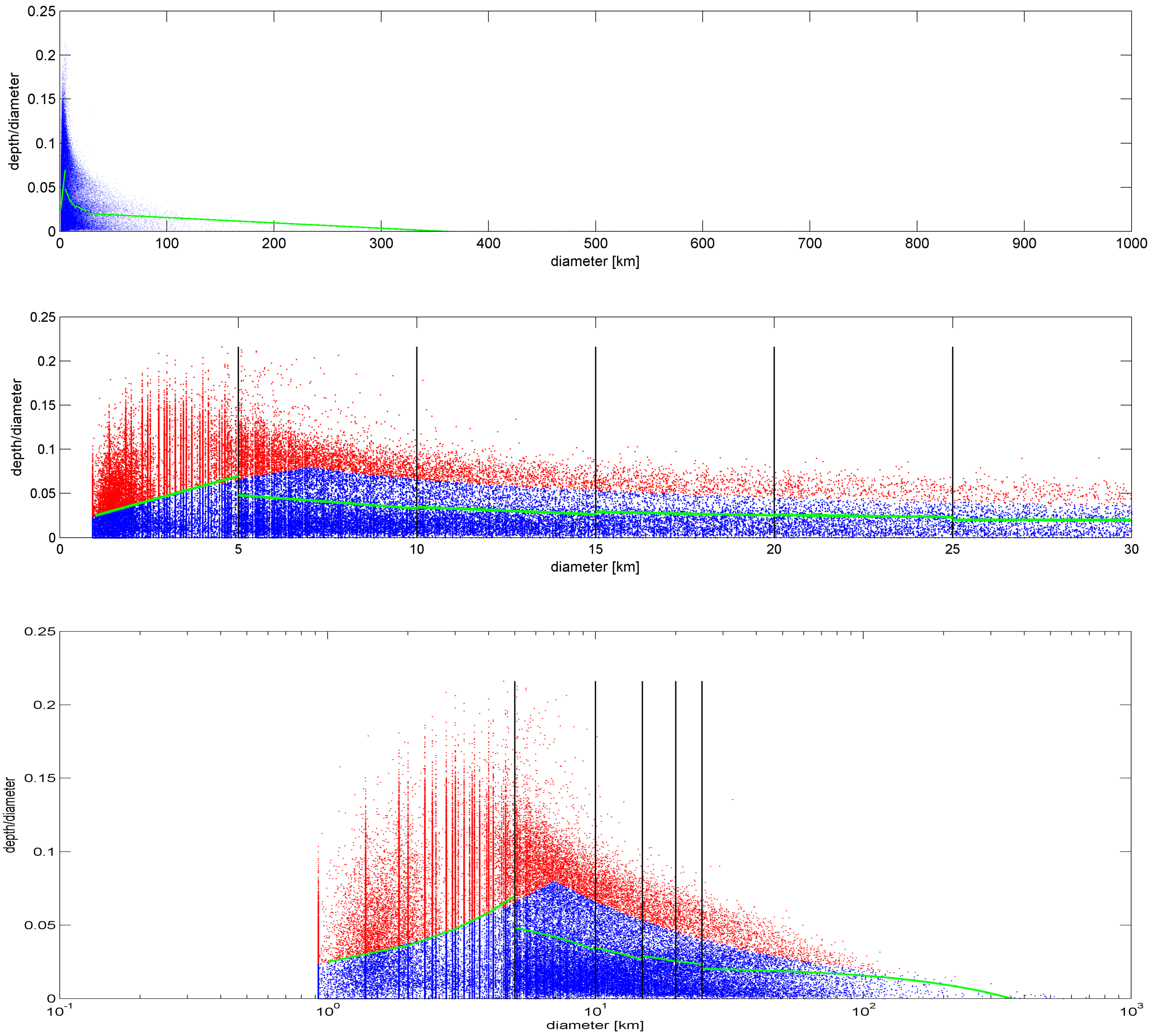

Figure 2.3: Distribution of depth/diameter against diameter of MA132843GT craters. Craters are divided into 6 bins according to their diameter ($5km < D$, $5km < D < 10km$, $10km < D < 15km$, $15km < D < 20km$, $20km < D < 25km$, $25km < D$). Blue and red dots (for shallow and deep craters respectively - all three plots) represent the craters, green lines are linear trends for each of the bins.

as the middle one, except for the diameter axis zoomed to 0-30km. Bottom figure shows the same distribution of depth/diameter against diameter of MA132843GT craters, but this time on a log-linear scale. As diameter of craters varies across three orders of magnitude and the majority of the craters have diameters¡100km it is convenient to show them in logarithmical scale.

2.2 Pristine craters

As was mentioned above, erosion processes trough time gradually decrease crater depth. Crater diameter, however, does not change, but mostly stays the same throughout its lifetime. To get a better idea of how this aging process affects crater properties we decided to create an artificial catalogue of pristine craters. Each crater in this new catalogue would retain its coordinates, diameter and surface type, but its depth (or rather depth/diameter) would be changed to that of a fresh crater of the same

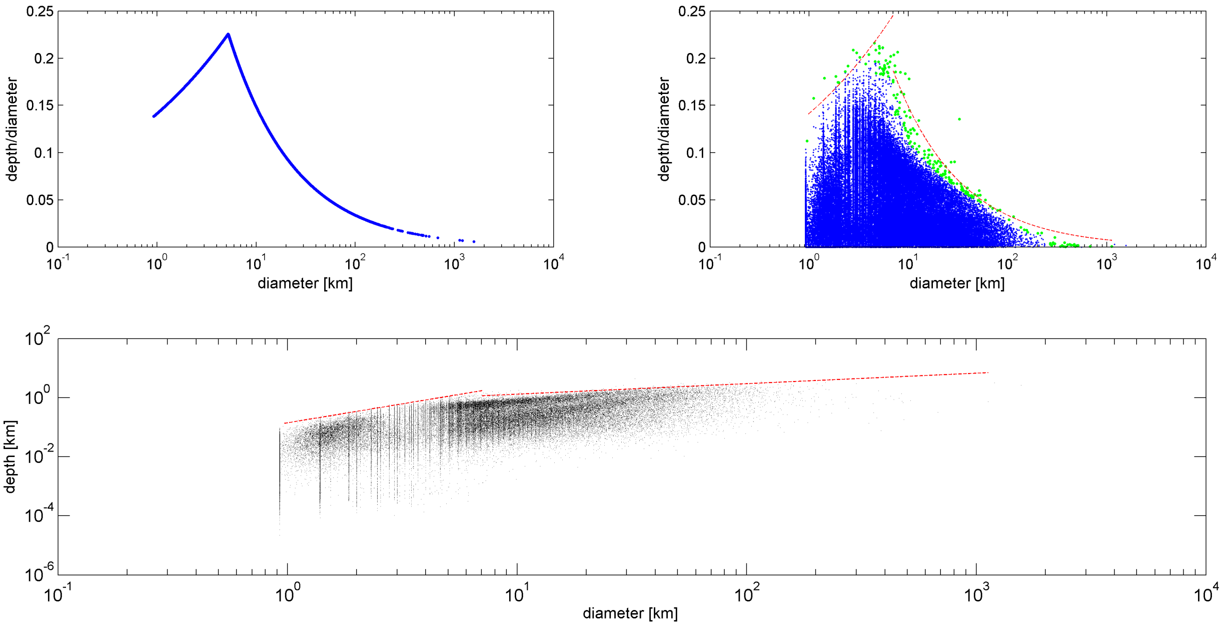

Figure 2.4: The catalogue of artificial pristine craters. From the MA132843GT catalogue (bottom panel - black dots, top right panel - blue and green dots) we selected craters with the highest depth/diameter ratio (d/D) for each diameter in the catalogue. These points represent the top of the distribution (top right panel - green dots). Two lines (bottom and top right panels - red lines) represent d/D of fresh craters. From this, a catalogue of pristine craters was created (top left panel).

diameter. Knowing that depth-diameter relationship corresponds to a power law, we proceeded to determine the analytical curve for the highest points in d/D vs. D distribution. We selected the highest d/D for every diameter and then selected data points on top of the distribution (Figure 2.4-top-right). After that we fitted the curve $d = a \cdot D^b$ trough these selected data points. Since the data clearly shows two different trends for simple and complex craters, we obtained different curves for craters with $D < 7km$ (simple craters) and $D \geq 7km$ (complex craters). For simple craters $d = 0.14 \cdot D^{1.28}$, while for complex craters $d = 0.66 \cdot D^{0.35}$. Verifying that these functions follow the crater distribution well, we can plot them in log-log scale as depth vs. diameter as in Figure 2.4-bottom. The final result is a catalogue of pristine craters with depth/diameter distribution as shown in Figure 2.4-top-left.

Chapter 3

Spatial distribution of craters

3.1 Latitude distribution

To get a better sense of global distribution of craters over Mars surface we will examine their depth/diameter distribution over latitude. The entire planet's surface is divided into three equal geographical zones (see Figure 2.1 for Martian map) according to their longitude coordinate: Zone 1 ($-180°$ to $-60°$), Zone 2 ($-60°$ to $60°$), Zone 3 ($60°$ to $180°$). Craters were also divided according to their diameter into six size bins, as described in section 2.1. Also, we plotted the shallow and deep craters in blue and red color respectively (Figure 3.1), to emphasize this two groups. Circles in figures that follow in this section represent depth/diameter trends and crater density according to latitude. They were calculated by binning the craters by latitude. Exact number of craters represented by each circle is shown in Table 3.1. This way horizontal distance between circles represents crater density for specific latitude range, while their relative vertical positioning indicates depth/diameter trends. It is important to notice that number of craters represented by each circle is different for each subplot. Main reason for this is a large difference in number of craters for each bin. If all of the circles were to represent the same number of craters on all of the subplots it would in some cases lead to either such a high number of circles that differences in horizontal density would be impossible to detect, or to such a low number of circles that it would be impossible to discern any trends. Previous similar work was done by Stepinski (2007), but only for the Terra Cimmeria region, while our analysis covers the entire Martian surface.

Studying the distribution also reveals some interesting features. Vast majority of the deep craters is situated between $-50°$ and $50°$ latitude. Shallow craters show a bit wider distribution to around $-75° - 75°$ latitude. As it would be expected, deep craters span a lot larger spectrum of d/D values. For zones 1 and 3 ($-180°$ to $-60°$ and $60°$ to $180°$) southern hemisphere has higher concentration of larger craters ($D > 5km$), while in zone 2 ($-60°$ to $60°$) craters are generally evenly distributed across latitude. Deep craters show an abrupt decrease in density around $\pm 40°$ latitude for all three zones while shallow craters show more uniform distribution.

3.2 Altitude distribution

Similar as with the latitude distribution, we analyzed how depth/diameter is distributed over altitude. Mars altitude is determined as a distance from the zero altitude level, which is determined as the level which has half of the planet's surface higher and half of the surface lower than it. The circles are again calculated by binning the data and calculating the average latitude and depth/diameter for all of the craters inside the bin to show data trends and the density of craters over certain altitude. The number of craters in each of the bins is displayed in Table 3.2. Though difference in altitude of the highest (20135m) and lowest (-8135m) crater is very high, most of the craters are located between -5000m and 5000m. There are no major differences in distribution between craters of different size bins (Figure 3.2). Small deep craters (first two bins) show a pronounced spike in depth/diameter ratio around -5000

Table 3.1: Number of craters represented by red (deep craters), blue (shallow craters) and black (artificial pristine craters) circles in Figure 3.1.

Bin	Zone 1 ($-180°$ to $-60°$)		
	Deep	Shallow	Pristine
$5km < D$	593.44	584	1204.75
$5km < D < 10km$	193.50	195.10	337.53
$10km < D < 15km$	86.75	84.88	156.25
$15km < D < 20km$	80	77.60	101.6
$20km < D < 25km$	46.66	47.30	87.57
$25km < D$	94.33	91.08	112.85
Bin	**Zone 2 ($-60°$ to $60°$)**		
	Deep	Shallow	Pristine
$5km < D$	694.05	682.50	1717.8
$5km < D < 10km$	222.13	222.63	497.41
$10km < D < 15km$	130.50	128.55	239.29
$15km < D < 20km$	100.67	100.20	164.09
$20km < D < 25km$	65	65.07	130.11
$25km < D$	144.50	143.22	242.77
Bin	**Zone 3 ($60°$ to $180°$)**		
	Deep	Shallow	Pristine
$5km < D$	723.44	728.08	1561.2
$5km < D < 10km$	191	190	463.75
$10km < D < 15km$	112	112.29	243.17
$15km < D < 20km$	94.33	96.69	140
$20km < D < 25km$	60.33	62.31	110.11
$25km < D$	110.50	110.88	193.92

m which cannot be seen in the distribution of larger craters. The altitude axis is cut-off at -9000 m and 9000 m to keep the graph centered, because crater densities above and below that are very low. The number of craters drops rapidly with size and so does the mean depth/diameter.

Interesting to note is that latitude distribution showed more variability between size bins. Maximum crater density is around 2000m altitude as can be seen individually for each of the bins (Figure 3.2) or for all of the craters together (Figure 3.3). Although maximum altitude on Mars is 20135m and the lowest altitude is -8135 m the altitude axis in Figure 3.3 shows -6000m to 7000m to get a better view of the distribution in the range of highest crater density. One other interesting feature of this distribution is that it seems that for small craters ($D < 5km$) there is a spike in depth/diameter around -4000m. This analysis was conducted for the whole Martian surface, not individual zones as latitude distribution. Detailed observation of altitude distribution dependence upon longitude would ask for a more detailed analysis of Martian surface features and their locations and could be a topic for further research.

3.3 Geographical distribution

We will now take a look at the spatial distribution of crater depth/diameter across the whole Martian surface. For a point on Martian surface we take a look at all of the crates in a $2°$ radius and that calculate their mean d/D. We do this for each of the six size bins discussed earlier. The results are shown in Figure 3.4. Color bar represents the scale for mean d/D. White color represents areas where there are no craters. Maps are shown in sinusoidal projection. It is the most suitable projection for

Table 3.2: Number of craters represented by red (deep craters), blue (shallow craters) and black (artificial pristine craters) circles in Figure 3.2.

	Deep	Shallow	Pristine
$5km < D$	1516.59	1522.20	3587
$5km < D < 10km$	808	804.55	1046.95
$10km < D < 15km$	285.80	291.91	542.86
$15km < D < 20km$	206.25	208	396.45
$20km < D < 25km$	172	173.77	277.5
$25km < D$	260.60	256.68	534.62

this purpose because it is an equal area projection. Since we are not interested in studying shapes and orientations of any surface features, having an accurate display of areas and sizes is therefore more useful. A similar analysis was performed by Stepinski (2010) and Stepinski (2007), except that they presented their results in a form of raster maps. They divided the surface of Mars into pixels of $0.5°$ in size and the value of d/D at each pixel was calculated as an average of the values of d/D for individual craters located within 2° square window centered at that pixel. If there are no craters, no values are assigned to that point. As expected, small craters are most abundant across the surface. Their density is highest in low and mid latitudes and slightly decreases towards the poles. Crater density is the highest for $5km < D < 10km$ bin, and interestingly it is the highest around equator to mid latitudes where it drops rather abruptly.

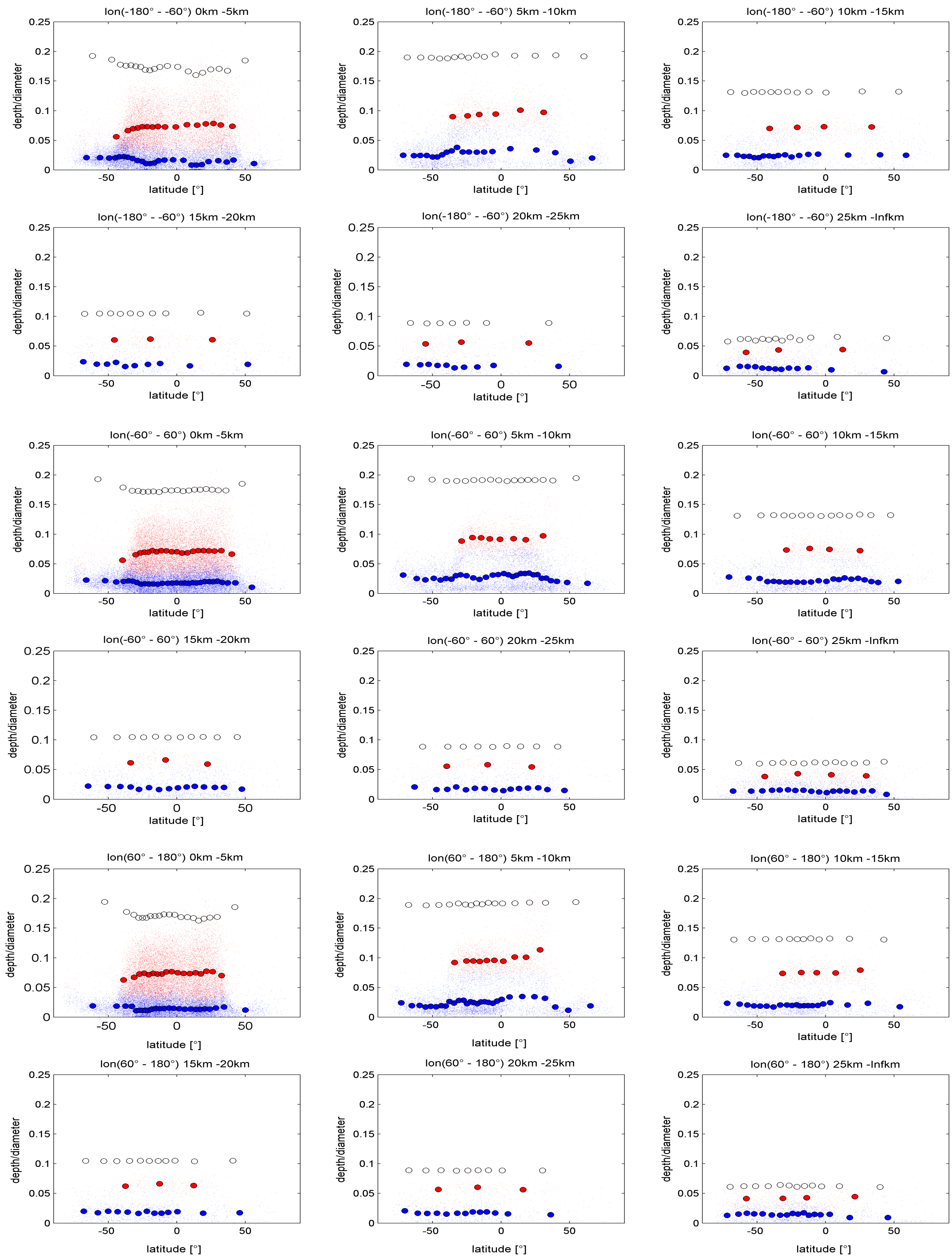

Figure 3.1: Depth/diameter against latitude for Martian craters (red dots and circles - deep craters, blue dots and circles - shallow craters, black circles - artificial pristine craters). In each of the zones craters are divided into bins according to their diameter and each bin is plotted separately. Circles are calculated by binning the data. In Table 3.1, a number of craters represented by each circle is given. Since the number of craters in every bin is not divisible by a whole number, some bins contain a rational number of craters. In practice that means that each circle contains a number of craters rounded up or down alternatively.

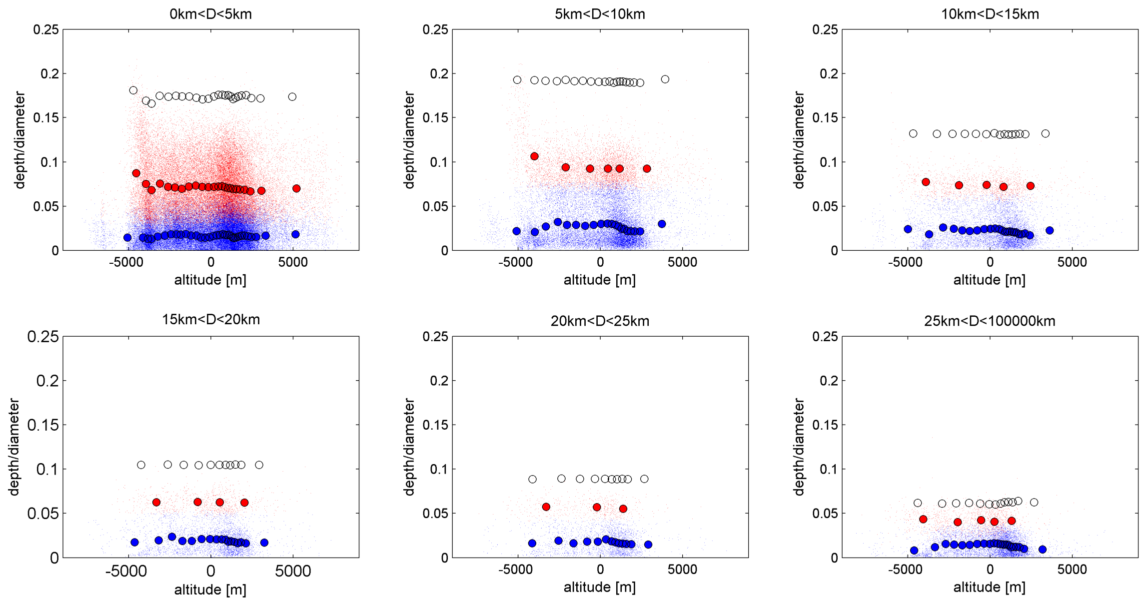

Figure 3.2: Depth/diameter against altitude (red dots and circles - deep craters, blue dots and circles - shallow craters, black circles - artificial pristine craters). The craters are divided into 6 bins according to the diameter (same as in Figure 3.1).

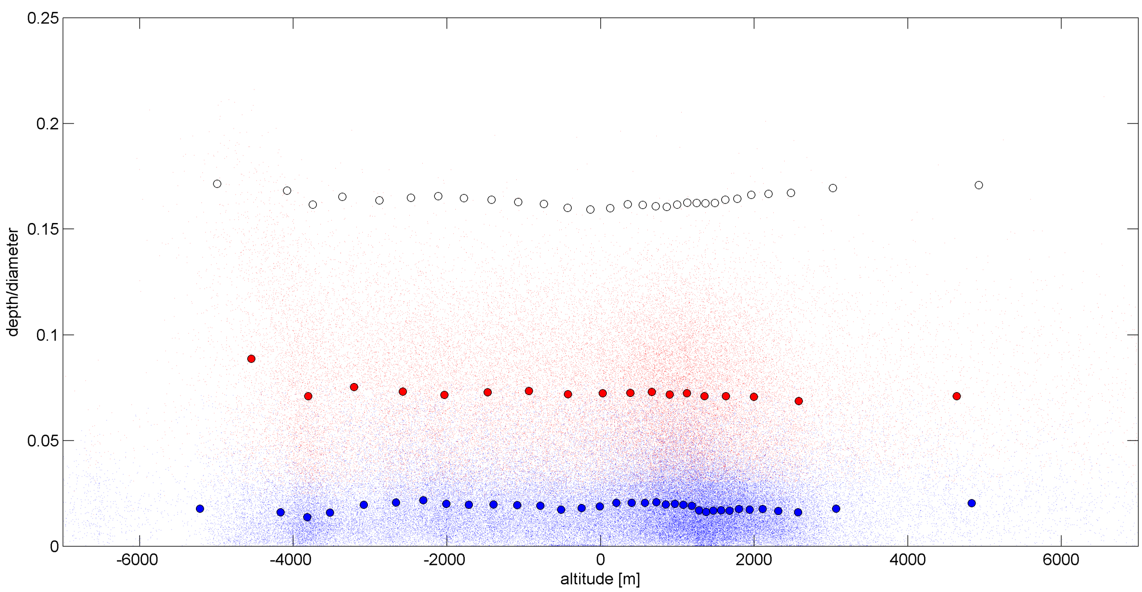

Figure 3.3: Depth/diameter against altitude for Martian craters. Unlike Figure 3.2 this figure shows all craters in one plot. Each red circle (deep craters) represents the mean altitude and depth/diameter of 2517.72 craters, each blue circle represents the mean altitude and depth/diameter of 2500.69 shallow craters and each black circle represents 4428.1 artificial pristine craters.

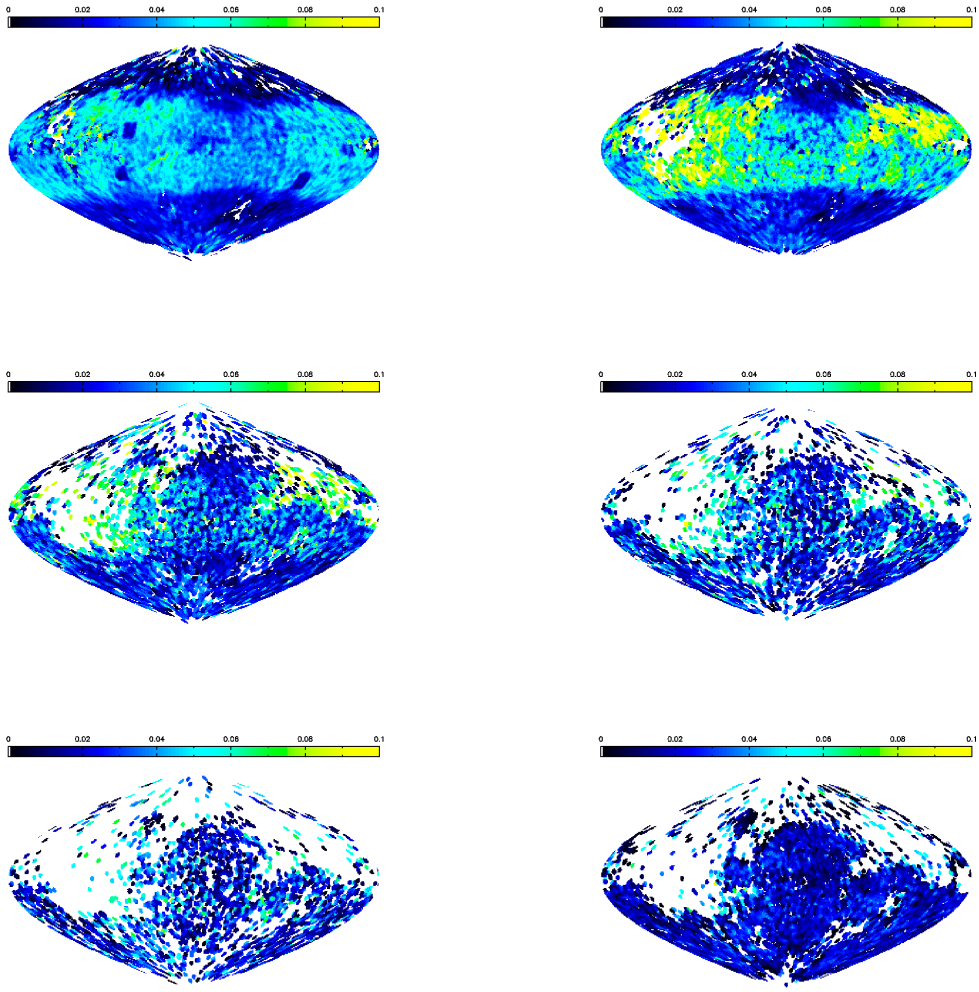

Figure 3.4: Geographical distribution of d/D on the surface of Mars for crater size bins: $D < 5km$ (89676 craters), $5km < D < 10km$ (20 940 craters), $10km < D < 15km$ (8144 craters), $15km < D < 20km$ (4362 craters), $20km < D < 25km$ (2776 craters), $25km < D$ (6951 craters). Values of this averaged d/D are shown in the color bar. White color shows regions without craters. Maps are shown in sinusoidal projection.

Chapter 4

Geological craters distribution

Since there are many different geological types of surfaces on Mars it is important to analyze differences and similarities in crater properties for various types of surface. There are three major geological eras identified in Martian history. First one was the Noachian (up to 3.5Gy ago), then Hesperian (3.5Gy - 2.9Gy) and the last Amazonian (2.9Gy - present) era (Tanaka, 1986). Since not every known surface type on Mars can yet be placed into one of these three eras, we will conduct analysis only for these four groups of surfaces. Also, some of the surfaces, either because of their small area or some other reasons, do not contain enough craters to make a meaningful statistical analysis. These surfaces have been excluded from further analysis.

We used the geological map by Skinner et. al. (2006). The surface codes are recoded with numbers for simpler handling as follows: *AHa=1, AHat=2, AHcf=3, AHh=4, AHpe=5, AHt=6, AHt3=7, Aa1=8, Aa2=9, Aa3=10, Aa4=11, Aa5=12, Aam=13, Aau=14, Ach=15, Achp=16, Achu=17, Ad=18, Adc=19, Adl=20, Ae=21, Ael1=22, Ael2=23, Ael3=24, Ael4=25, Ah4=26, Ah5=27, Ah6=28, Ah7=29, Ah8=30, Am=31, Aml=32, Amm=33, Amu=34, Aoa1=35, Aoa2=36, Aoa3=37, Aoa4=38, Aop=39, Aos=40, Api=41, Apk=42, Apl=43, Aps=44, As=45, At4=46, At5=47, At6=48, Avf=49, HNu=50, Had=51, Hal=52, Hap=53, Hch=54, Hchp=55, Hcht=56, Hdl=57, Hdu=58, Hf=59, Hh2=60, Hh3=61, Hhet=62, Hpl3=63, Hplm=64, Hr=65, Hs=66, Hsl=67, Hsu=68, Ht1=69, Ht2=70, Htl=71, Htm=72, Htu=73, Hvg=74, Hvk=75, Hvl=76, Hvm=77, Hvr=78, Nb=79, Nf=80, Nh1=81, Nm =82, Npl1=83, Npl2=84, Npld=85, Nple=86, Nplh=87, Nplr=88, b=89, cb=90, cs=91, d=92, m=93, s=94, v=95.*

The complete list of all the surfaces in Noachian, Hesperian and Amazonian group, as well as those of unknown age and the excluded surfaces can be found in Table 4.1. The first three groups will consist of surfaces whose age have been determined and therefore can be placed into one of the eras. Fourth group will consist of surfaces whose age is still unknown. The list of surfaces divided by eras they belong to is shown in Table 4.1

For these three groups, as well as individual surfaces we will take a look at their crater density distributions as it relates to crater's d/D. Crater density can be calculated in two different ways: as absolute density and as relative density. Absolute density is simply determined by counting all the craters on a specific surface and dividing the number by the surface area. That way we get absolute crater density for a specific surface expressed in $\frac{N}{deg^2}$. Relative density is determined by taking all of the craters in a specific d/D bin and calculating the percentage of those craters which can be found on that specific surface.

4.1 Crater count

Crater counting with isochrones can be used as an effective method to determine the age of the surface. While it is not very precise, it is reliable enough to determine the age within the order of magnitude, which at the current level of Mars's surface exploration is good enough. We determine the approximate age of a surface by plotting the cumulative crater frequency per km^2 against crater diameter. This

Table 4.1: Martian surfaces divided according to their age. Each era has surfaces listed by their number designation (Skinner et. al., 2006, , see text). Group labeled "The rest" contains surfaces used in analysis whose age is still unknown. The last group labeled "Excluded surfaces" lists surfaces that have been excluded from further analysis for lack of crater data.

Era	Number designation of the surface									
Noachian	83	84	85	86	87	88				
Hesperian	5	56	63	65	66	74	78			
Amazonian	10	11	17	22	24	32	33	42	44	54
The rest	3	7	13	14	39	46	47	48	52	55
	59	67	68	70	73	80	90	91	94	95
Excluded surfaces	1-2	4	6	8-9	12	15-16	18-21	23	25-31	34-39
	40-41	43	45	49-51	53-54	57-58	60-62	64	69	
	71-72	75-77	79	81-82	89	92-93				

makes isochrones, in fact, size distribution lines that correspond to various geological ages. Martian isochrones were derived from crater production function (Ivanov et.al., 2001) and the chronology function (Hartmann, Neukum, 2001), by comparing with Moon data and using the cratering ratio between Mars and Moon. Cumulative crater frequency is calculated as the sum of number of craters in a bin of particular diameter and the number of craters in all bins of greater diameter, as recommended by standard cratering analysis techniques (Standard Techniques for Presentation and Analysis of Crater Data, 2001) (Figure 4.1).

4.2 Relative distribution of craters

As mentioned before we will take a look at relative crater distributions for various Martian surface types. Relative distributions are calculated as a percentage of craters in a certain d/D bin that belongs to a particular surface. The percentage was calculated as the percentage of all of the craters in certain d/D bin that can be found on that particular surface. Surfaces which do not have at least 2% craters in at least one of the bins are not displayed. Since the highest $d/D \approx 0.2$ we decided to divide craters into 19 bins with $\Delta d/D = 0.01$ step size, with the last bin containing all craters with $d/D \geq 0.18$.

We then grouped the geological surfaces by using their mean linear fit as a discriminating factor in the following way. For each surface distribution profile we calculated the coefficients a and b in $y = ax + b$ linear fit equation. Then we divided them based on whether their linear trend was growing, falling or near constant. To determine which trends are near constant we found maximum absolute value of a among all surfaces and we set the condition $|a_{Group2}| \leq 0.1 \cdot |a|_{max}$. This is called Group2 and it contains surfaces that follow a linear trend. Group1 consists of surfaces with $a_{Group1} < -0.1 \cdot |a|_{max}$ and Group3 consists of trends $a_{Group3} > 0.1 \cdot |a|_{max}$. Figure 4.2 shows plots of each group along with their mean profile and mean linear trend. Only surfaces with at least one data point above 2% were plotted. We can see that Group1 overall has the highest crater percentages, while Group2 and Group3 are similar in shape for shallow craters $d/D < 0.1$ and start to differ for deeper craters. These differences are probably due to the fact that the shallower craters are often larger and thus fewer in numbers. The majority of the craters have $D < 10km$ and smaller craters not only tend to be deeper but they are also more frequent, so their distribution among the surfaces would be more uniform.

When we take a look at the relative distribution profiles grouped by age, some interesting features emerge (Figure 4.3). Most of the surfaces in Group1 belong to Noachian age, the oldest geological era on Mars. This is consistent with what would be expected, as older surfaces have more time to accumulate craters, but smaller craters also get eroded and filled with material so they disappear leaving only the bigger shallow ones. As we look at geologically younger surfaces (Hesperian and Amazonian

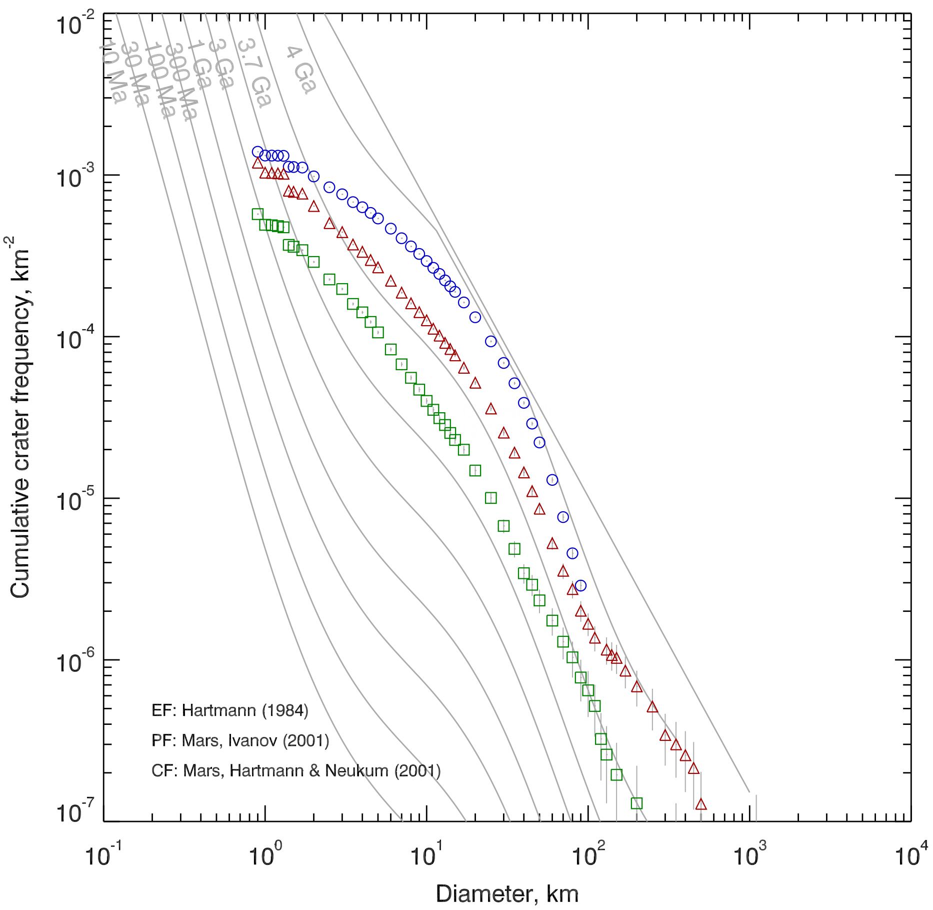

Figure 4.1: Isochrones lines of Martian surfaces. Black curves represent isochrones of the same age. The straight black line represents the saturation boundary, i.e. the maximum crater density for a given diameter (Hartmann, 1984). The isochrones are derived from knowing the crater production function (Ivanov et.al., 2001) and the chronology function (Hartmann, Neukum, 2001). Colored data points are mean crater densities for different Martian surfaces. Blue circles represent Noachian surfaces, red triangles represent Hesperian era surfaces and green squares represent Amazonian age surfaces (Skinner et. al., 2006).

age) we notice more profiles from Group3. From mean profiles as well as from groupings of surfaces we can see that for the oldest surfaces there are higher percentages of shallow craters. Noachian mean profile shows larger concentrations of shallow eroded craters, while Hesperian and Amazonian show larger percentages of deeper, fresh craters. Hesperian surfaces profile represents a sort of transitional profile between Noachian and Amazonian. This is to be expected since older surfaces are more likely to hold older craters which have had more time to erode. Younger surfaces had less time to accumulate craters, so that most of them are smaller ones that are more frequent. And since the surface is younger,

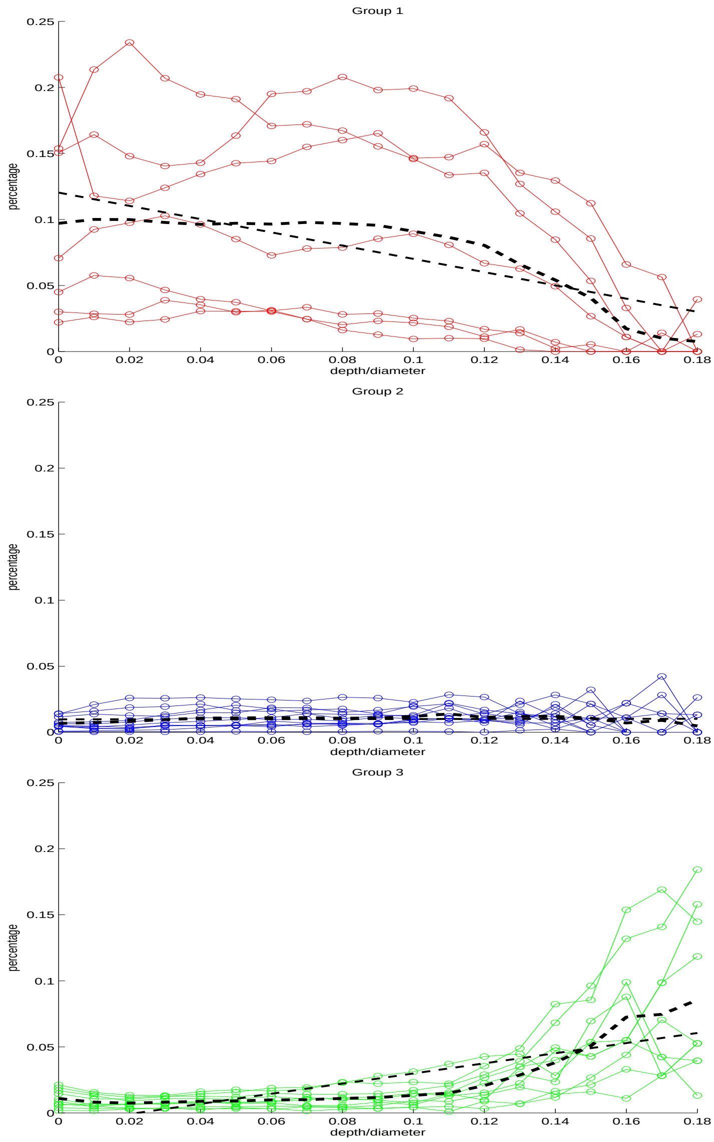

Figure 4.2: Crater percentage profiles for geological surfaces. Profiles are fitted to the linear function $y = ax + b$ and then grouped based on their parameter a. The thicker black curve on all three graphs is the mean profile for that group and thinner dashed line is the linear trend of the mean profile.

there was not enough time for erosion to erase the impact structures from the surface. Comparing this with Figure 4.2 we can see that Noachian group is comprised mostly of craters in the Group1 in Figure 4.2, while Amazonian group is more similar to the Group3. Hesperian group is partially made of both of those. Surfaces of Group2 in Figure 4.2 seem to be evenly distributed in all four of these groups. These differences can also be seen by looking at the mean profiles of surface distributions.

4.3 Absolute distribution of craters

After analyzing relative crater distributions we will take a look at absolute distributions. Absolute distribution is actually crater density function expressed in $\frac{N}{deg^2}$ for a particular d/D bin. It is calculated by expression $\eta_j^i = \frac{N_j^i}{A^i}$ where N_j^i is the number of craters in j^{th} bin and on i^{th} surface and A^i is the

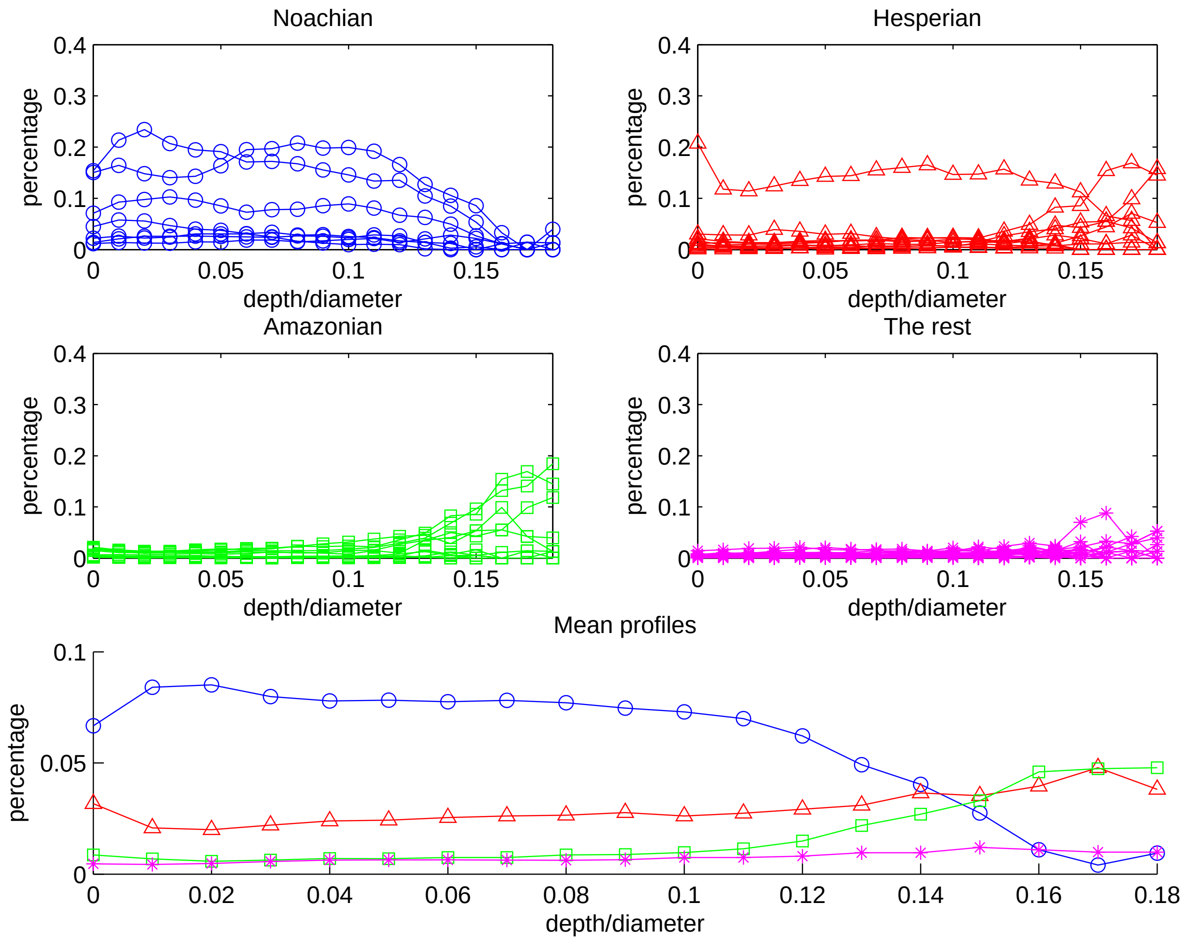

Figure 4.3: Crater percentage profiles for Martian surfaces divided according to age. Top left graph are surfaces of Noachian era (blue circles), top right are surfaces that belong to Hesperian era (red triangles), middle left are surfaces of Amazonian era (green squares) and middle right are the rest of the surfaces whose age is still unknown (magenta stars). The bottom graph represents the mean profiles for each of the groups.

area of i^{th} surface type in deg^2. These bins are arranged in the same way as in relative distribution calculations. Crater densities, unlike relative distributions, show for each surface higher concentrations of shallow craters and negative trends as d/D increases (Figure 4.4). This can be attributed to the fact that shallow craters are much more abundant than deep, as shallow craters cover the whole range of crater diameters while higher d/D can only be found for smaller craters.

Out of 95 different geological surface types on Mars we selected only the ones which have enough craters to have at least 8 data points. For each surface we determined two fit functions, one for $d/D \leq 0.11$, the other for $d/D \geq 0.11$. The general functions form is $y = C \cdot 10^{ax}$. We see some differences in these two parts of distribution. If we take a look at individual surfaces it is useful to compare their density profiles with our catalogue of pristine craters to get a better impression of how craters erode (Figure 4.5). Real craters accumulated trough time have higher densities of shallow craters while some surfaces have no deep craters at all. If we take a look at missing data points we can see that there are no data points missing for $d/D < 0.07$ and most of the zero densities can be found for $d/D > 0.11$. Observing the density profiles and by studying the cratering process we expect the distribution to scale as an exponential function. Linear fits made to density distribution profiles are lines $y = ax + b$ in logarithmical scale, which makes them exponential functions $y = 10^{ax+b}$ in linear scale. Two distinct

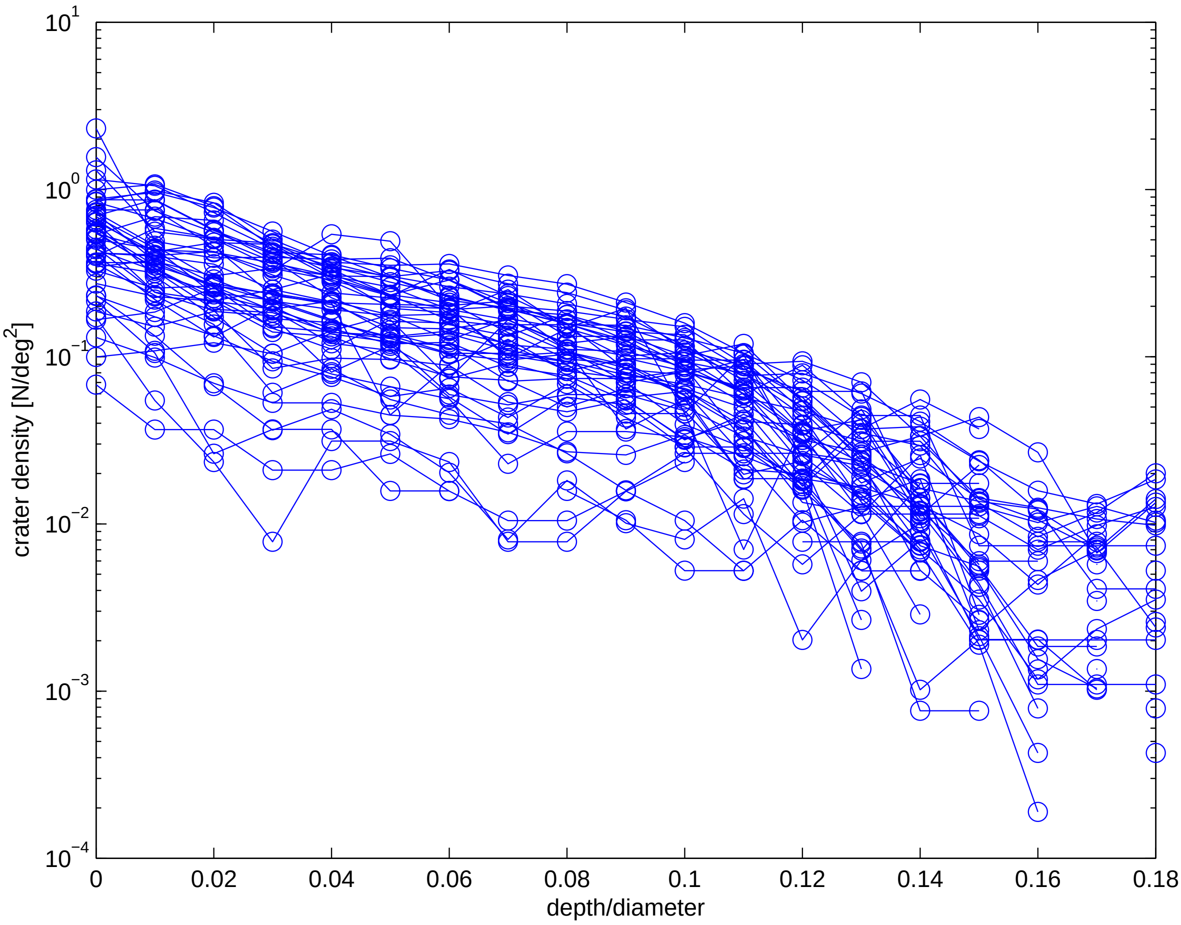

Figure 4.4: Surface density profiles. Surface density for each of the 95 types of surfaces on Mars The figure is plotted in log-linear scale for the trends in density profiles to be clearer.

trends can be observed in surface density profiles. One for $0 < d/D \leq 0.11$ and the other one for $d/D \geq 0.11$. Detailed method for fitting the data is described in Figure 4.10.

Complex and simple craters also show differences in density distribution. Simple craters are more abundant, with maximum crater density at 10^0 while for complex craters maximum density is 10^{-1}. Also, complex craters show enough data points on 5 surfaces (Figure 4.7), while simple craters have enough data points on 45 Martian surfaces (Figure 4.6) to make meaningful data fits and analysis. This difference in crater abundance could be the reason for differences in profile shapes. Simple craters show more even distribution with very similar slopes between two fit functions, while complex craters show more uneven distribution with much more changing slopes and even some profile with higher densities for mid range d/D bins ($0.4 < d/D < 0.12$) than for lower d/D values.

Not all of the surfaces represented in Figure 4.5 are represented in Figures 4.6 and 4.7. It is because only the surfaces with enough data points (at least 8) have been selected. Although the most of the Martian craters are simple, they are not equally abundant on all of the surface types. Since complex craters make up smaller amount of the total number of craters their density is high enough on even fewer surfaces than the simple craters.

Similar as with relative distributions we can take a look at some common features of density distributions when we group them according to their surface age (Figure 4.8). If we observe the Amazonian, Hesperian and Noachian group, we can see how surface crater density evolves trough time, increasing number of shallow craters and decreasing the number of deep craters. Younger surfaces show greater variability in distribution, while for older surfaces the distribution curves show very little dispersion. The curve slope decreases trough time as erosion decreases crater depth. For the group of surfaces of unknown age, we can see profiles similar to those of all of the other three groups. The case is similar if we make individual analysis for simple and complex craters (Figure 4.9). By grouping the profiles this way we can see how complex craters lack the deep crater population in all of the groups. In fact, complex craters have much lower crater densities (or no craters at all) for $d/D > 0.11$. This is consistent with crater formation process, where we know that initial depth/diameter of the complex craters is smaller than that of simple ones and trough erosion that ratio can only decrease. This makes it obvious that this is not a consequence of erosion or redeposition of material, but an intrinsic property of complex craters, which comes from their formation process mechanics and their size. Overall shape of the distribution curves remains similar for complex and simple craters, but simple craters show much greater differences in crater densities between the data curves.

The two fit functions that were calculated for each surface provide us with more insight into changes that occur in density profile of a surface as it gets older. The fit functions have general expression $y = C \cdot 10^{ax}$ where $C = 10^b$. Figure 4.11 shows scatter plots of coefficients $a1$ and $a2$ as explained in Figure 4.10. Top four graphs show $a1$ vs. $a2$ coefficients for different surface groups divided according to age (Noachian - oldest age, Hesperian - middle age, Amazonian - youngest age, and the ones that are yet undetermined). Colored stars represent real data and squares represent pristine craters. Bottom two figures show enlarged version of the top four. On the left bottom figure all of the coefficients for Noachian (circles), Hesperian (squares) and Amazonian (triangles) surfaces are plotted together. Colored symbols represent real data and black ones represent pristine craters. The difference between

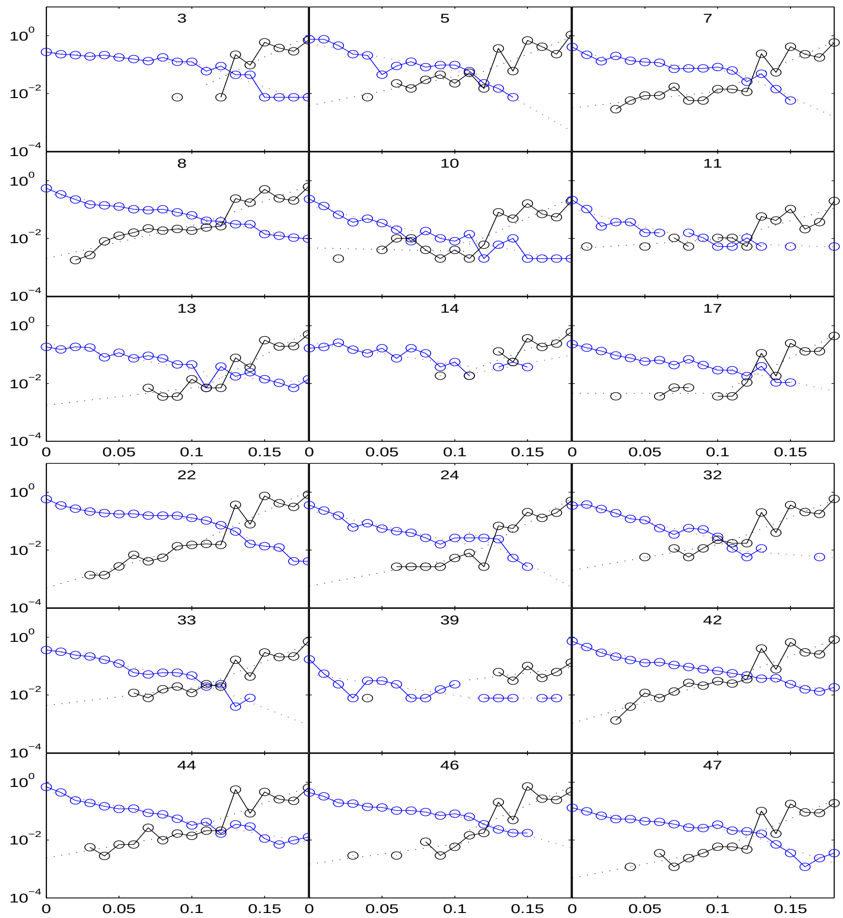

Figure 4.5:

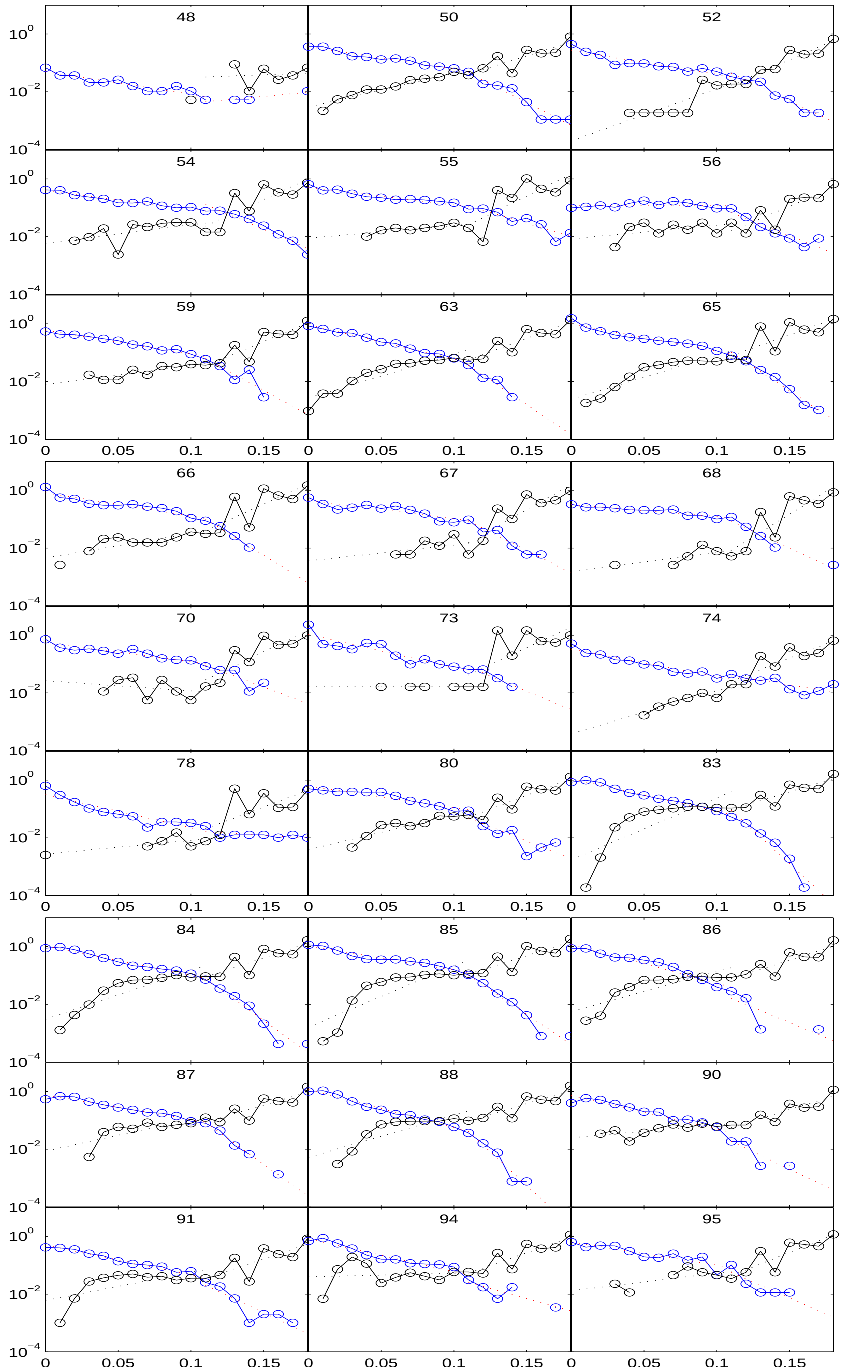

Figure 4.5: Surface densities for different Martian surface types. The x-axis represents depth/diameter bins, the y-axis represents crater density in N/deg^2. Data is represented by blue circles and data fit functions are represented by red dotted line. Black circles and black dotted line represent density for pristine craters and their linear fits respectively.

real data and pristine craters with no erosion is very well shown here. When plotted together (Figure 4.11 bottom left) it is clear how $a1$ changes very little trough the aging of a surface. The $a1$ and $a2$ coefficients for real data are negative and their distribution shows that $a1$ varies very little. In fact it stays almost the same for all of the groups and surfaces, always between -20 and 0. The $a2$ varies a lot and its variation shows the evolution of surfaces trough time. For oldest surfaces $a2$ is the lowest

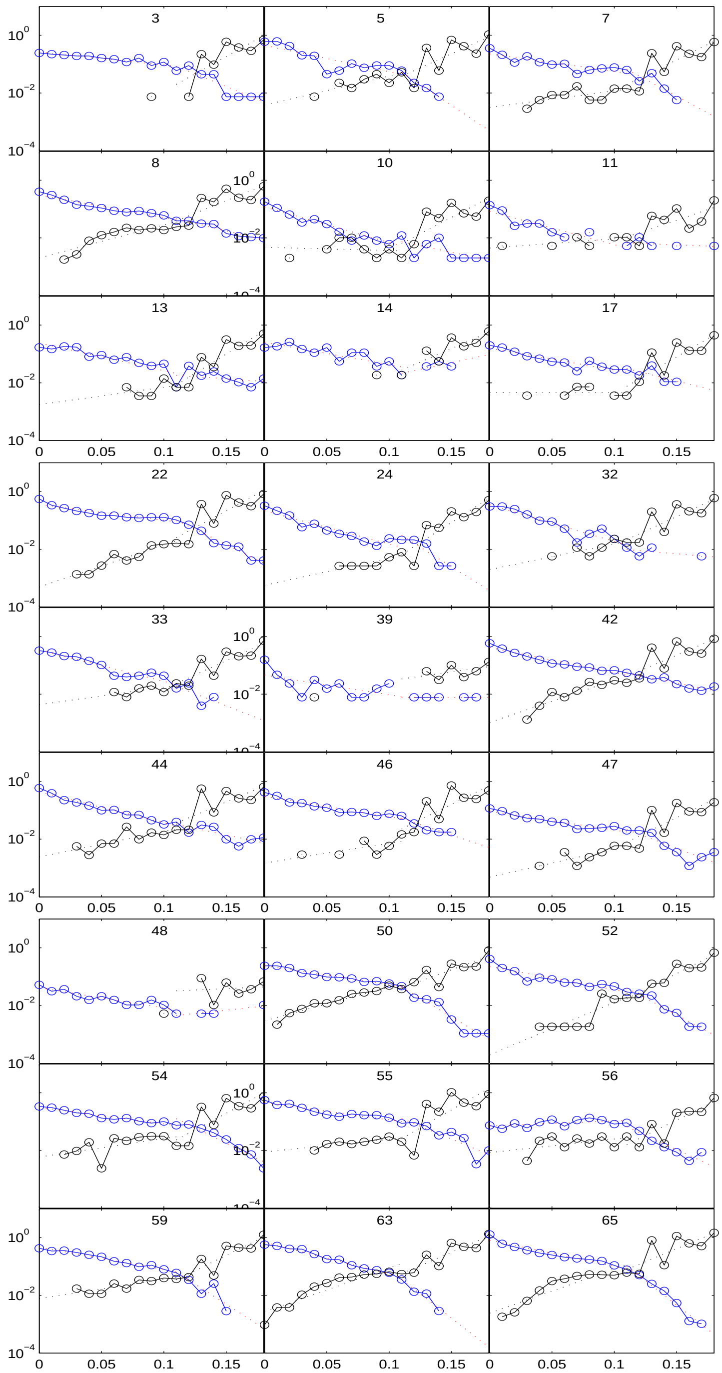

Figure 4.6:

(mostly -50 to -35 with one exception at -20). Middle aged Hesperian surfaces take up middle range and they vary a lot (-35 to 0), while the youngest surfaces have the highest $a2$ coefficients (-30 to 0). This is because $a1$ is part of the fit which describes shallow craters and they are either already eroded or were formed as very shallow so they do not change very much over time. On the other hand, $a2$ decreases as we look at older surfaces. This means that with the passage of time number of deep craters on a surface decreases and so does their density. As the surface gets older this decrease is visible in increasing negative slope of fit function which describes the deep craters. If we take a look at pristine craters (black data points in Figure 4.11) we will notice that when we remove the effects of erosion on

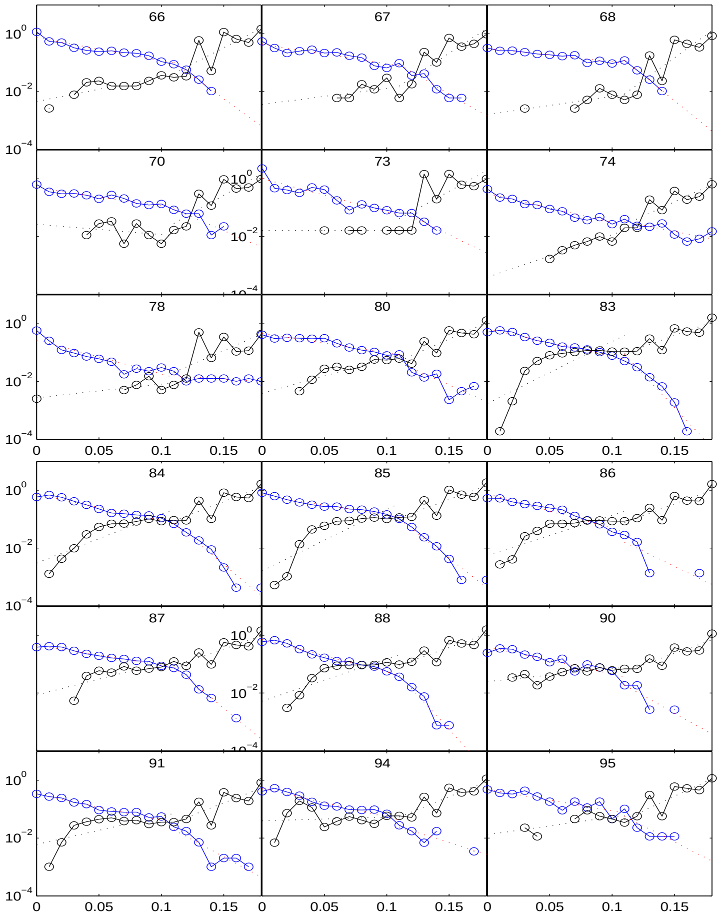

Figure 4.6: Surface densities for simple craters ($D < 7km$). Blue circles connected with line represent the surface density, red dashed line represents fitting curves (Figure 4.10) and black dashed line with circles represents surface density for pristine craters.

craters that all of the randomly scattered within a narrow range of values. This leads to conclusion that surface age (trough craters erosion) is the main influence in the slope of the crater density profiles of Martian surfaces. All of the pristine crater coefficient are positive and they are all mixed together as they represent an ideal case of crater distribution with no erosion, and consequently no surface evolution trough time. The undivided surfaces show a wide range of values indicating they are both older and younger surface types in that group.

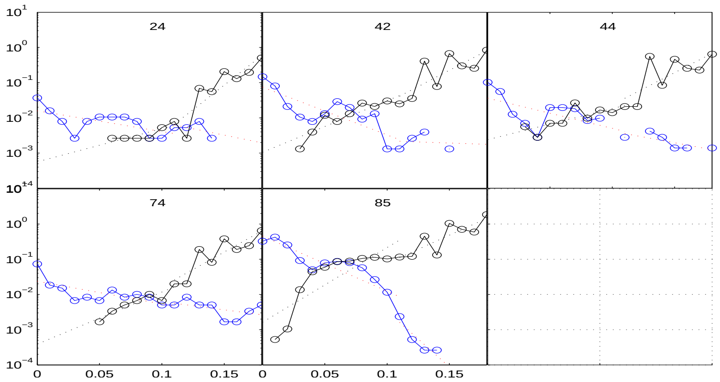

Figure 4.7: Surface densities for complex craters ($D \geq 7km$). Blue circles connected with line represent the surface density, red dashed line represents fitting curves (Figure 4.10) and black dashed line with circles represents surface density for pristine craters.

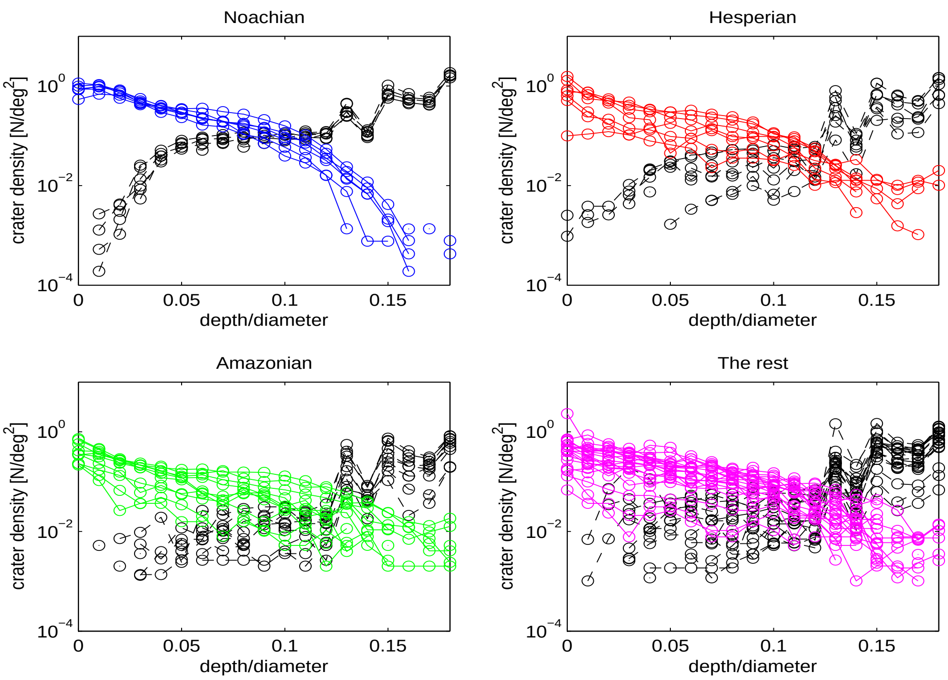

Figure 4.8: The division of surface density profiles according to their age. Colored circles represent data points. Black lines and circles represent the density distribution of artificial pristine craters for each of the surfaces.

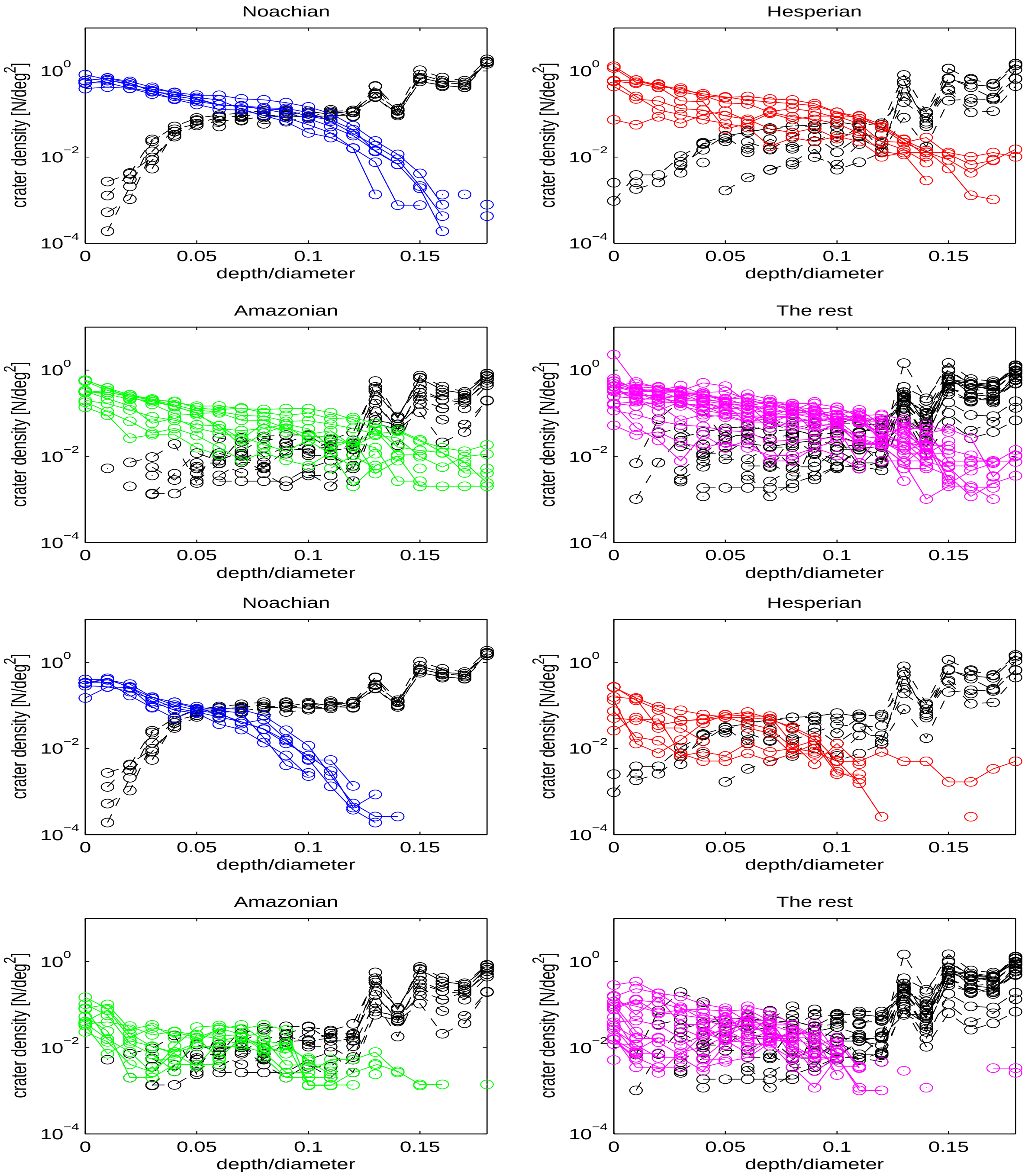

Figure 4.9: Surface density profiles divided by age for complex ($D \geq 7km$-bottom 4 graphs) and simple ($D < 7km$-top 4 graphs) craters. Colored circles represent data points. Black lines and circles represent the density distribution of artificial pristine craters for each of the surfaces.

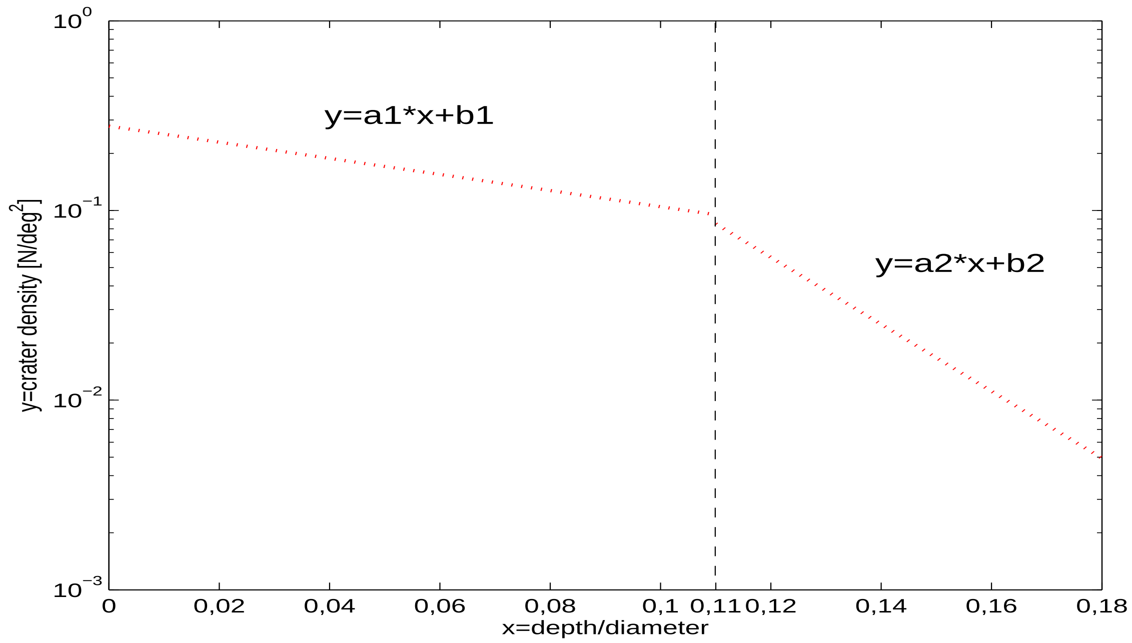

Figure 4.10: Linear fits in linear-log scale. Most of our surface densities have a noticeable change in slope around x=0.11 - 0.12. for that reason we decided to fit two lines for every surface density distribution. One for $d/D \leq 0.11$ and one for $d/D \geq 0.11$. In linear scale this becomes the $y = 10^{ax+b}$ exponential function.

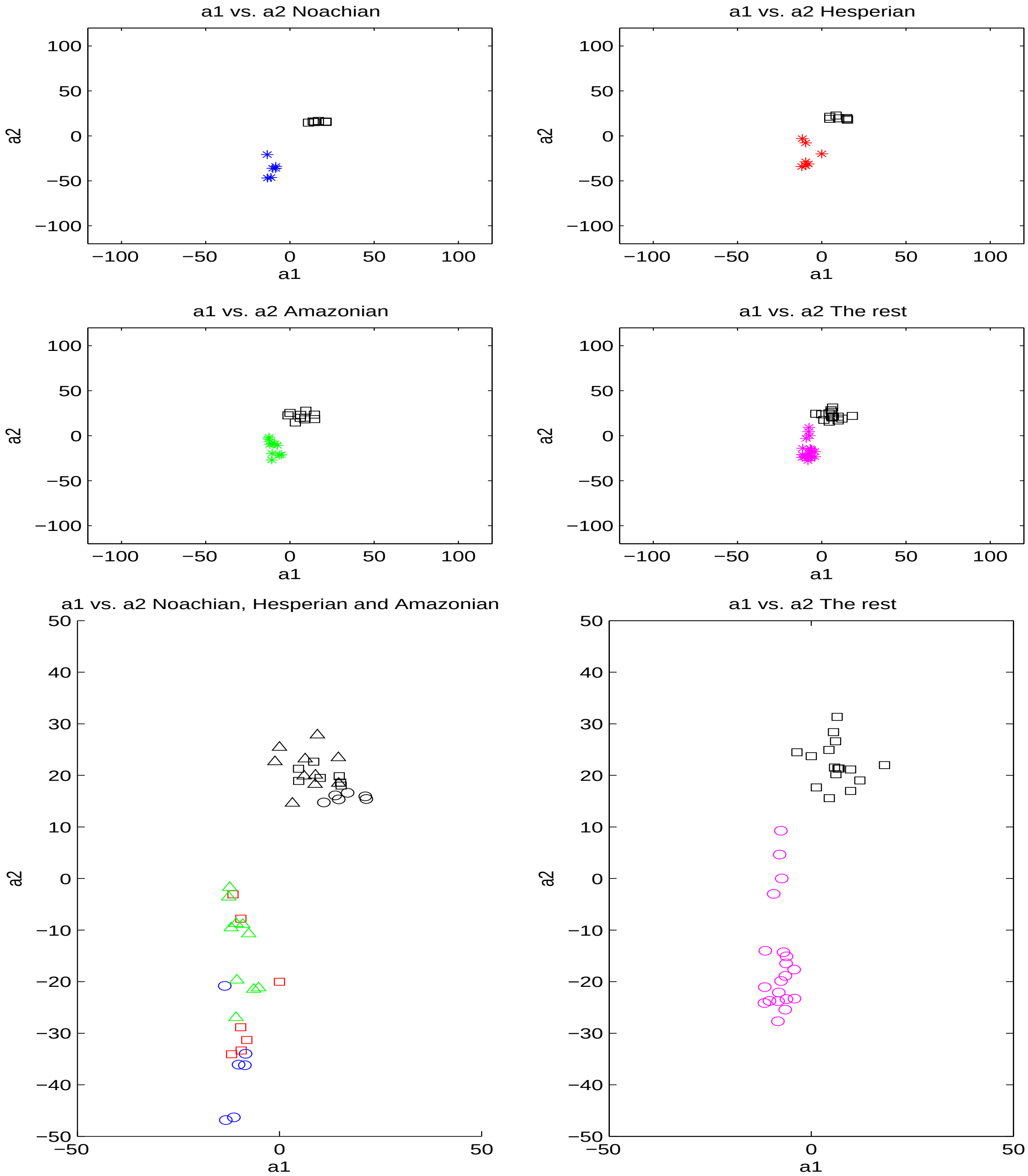

Figure 4.11: Scatter plot for a and b coefficients in fit functions for surface densities (Figure 4.10). Blue circles - Noachian surfaces, red squares - Hesperian surfaces, green triangles - Amazonian surfaces. Black symbols represent the pristine craters.

Chapter 5

Discussion

The new Martian craters catalogue MA132843 provides a lot of new data for study of statistical properties and distributions of Martian craters. For a large scale analysis it is best to characterize crater morphology with two main attributes: their depth d and their diameter D and their ratio d/D. Using this ratio we can categorize the craters as deep or shallow depending on their diameter and their depth/diameter ratio (Figure 2.2). When plotted against each other in logarithmical scale, we can notice an upper limit to the depth of a crater for a specific diameter (Figure 2.3). This upper limit is actually the depth of freshly formed craters. When plotted for the whole range of diameters a pattern emerges, so it is possible to determine the functional relation of depth and diameter for fresh craters (Figure 2.4). Form these data it is possible to construct the artificial catalogue of fresh craters assigning those depths they had when they were freshly formed.

The craters distribution across the Martian latitude is generally uniform. There are some differences in the distribution of deep and shallow craters. Analysis shows significant number of shallow craters in high latitudes (up to $\pm 70°$), while deep craters are located mostly within $\pm 50°$. This is most probably a signature of variable cryosphere depth (Schwenzer et al., 2012) or relatively more abundant number of impactors coming from the ecliptic. Altitude distributions on the other hand do not show these kinds of differences. Both shallow and deep craters exhibit almost the same distribution along the altitude. Different size bins of craters have shown no significant differences in their distributions as well. When we take a look at the crater distribution along the longitude we can see that they are mostly uniformly distributed (Figure 3.4). There are, of course, areas with higher density of craters on Martian surface, especially for the larger size bins which contain fewer craters.

Crater counting provides us with a sort of checkpoint for our analysis of crater distributions for different age groups. Due to the resolution problems for small craters ($D \leq 2km$) this analysis cannot be used as a precision tool, but rather as an estimate on a Gy scale. The curves for each of the groups correspond roughly to the ages of the respective periods as they were determined in ((Tanaka, 1986)). Due to the very different nature of the surfaces of unknown age there is no point in calculating their mean profiles. More detailed analysis for each surface individually is needed determine their ages.

In analyzing the relative distributions of craters we find that the distribution's shape generally corresponds to the age of the surface in question. Relative distributions are calculated as a percentage of craters of a particular d/D bin present on a specific surface. This gives us a good basis for the comparison of surfaces and their crater population. Surfaces are divided into three groups according to linear trends of their relative distributions (Figure 4.2). When we group those surfaces and their relative distribution profiles according to age, we notice that older surfaces (Noachian age) have relative distributions with higher percentages for shallow craters and a drop in the abundance of deeper craters. Younger surfaces (Hesperian and Amazonian age), show distributions with higher parts of deep craters (Figure 4.3). These results fit the expectations for this kind of analysis as older surfaces are more likely to acquire more shallow craters trough time, be it from large impacts which are by nature of cratering process more shallow, or trough erosion of deep craters. As large impacts are less common than smaller ones, younger surfaces have had less chance to accumulate large complex (and thusly shallow) craters. Their crater population consists mostly of smaller craters and since the surfaces are younger in origin, for most of them there has not been enough time for erosion to decrease their depth. Hence, for deeper craters there is a greater possibility to find them on a geologically younger surface.

Absolute crater density distributions provide us with another type of information about the surfaces. Crater densities are expressed as number of craters per degrees squared ($\frac{N}{deg^2}$). General shape of the profiles leads us to conclude that we can fit them with two exponential curves, one for deep and one for shallow part of the d/D bins (Figure 4.10). Analysis of the profiles for simple and complex craters confirms what would be expected knowing their attributes. Simple craters show higher densities for deep craters and lower densities for shallow craters than complex ones for the same surface. It is important to note that when we look at individual profiles, either for simple and complex craters or for all craters on one surface, there are always higher densities of shallow craters than the deep ones. If we compare this with pristine catalogue (Figure 4.5) we can assume that the main reason for such trends is erosion and natural decay of the craters walls which all work to decrease the crater's depth and slowly bury it. Pristine craters show much higher densities for deep craters as that catalogue assigns crater depths as those that would exist when the crater was freshly formed. Since majority of craters are small simple craters which tend to be deeper that the large complex ones, those smaller craters would have higher densities. Looking at the same profiles grouped by age we only confirm this observation (Figure 4.8). The older the surface gets, the lower densities are for the deep craters. Noachian age surfaces do not even have any craters of the deepest d/D bins. Analysis of the fitting functions shows that the first fit function (for shallow craters) does not change very much for different age groups (Figure 4.11). The second part of the fit however changes its slope significantly as the surface ages. As it gets older, the slope becomes more negative as erosion makes the craters shallower.

Chapter 6

Conclusion

With new MA132843GT catalogue, we get a chance to study global statistical properties of Martian craters. We examined some general characteristics of craters and their morphological parameters, as well as their spatial distribution over Martian surface. Crater's diameter and depth/diameter ratio are taken as the best way to describe its morphological properties. That way it is possible to distinguish small, large, simple, complex, deep and shallow (which usually means fresh and old) craters. Trough the creation of the catalogue of artificial pristine craters we found the power law dependence of d/D to diameter for fresh craters. These results can be made more precise trough comparison with craters on other Solar system bodies and trough experimental methods (Salamunićcar et al., 2012).

Spatial distribution of craters and their latitude distribution reveals some interesting features and differences between shallow and deep craters and between different crater size bins. A more detailed analysis can be made for smaller areas on the surface, possibly with higher resolution data to identify multiple impact regions or previously unknown small craters.

Distribution profiles and crater counting techniques make a connection between crater density and their d/D. These profiles (the relative and absolute ones) show dependence with the age of the surface they are on. Since there are still many surface types on Mars whose age is still unknown, studying these profiles can help in further dating the rest of the Martian geological surfaces.

Bibliography

Crater Analysis Techniques Working Group, 1979, Icarus, 96, 165

Hartmann, W., F., 1984, Icarus, 60, 56

Hartmann, W., F., Neukum, G., 2001, Space Science Reviews, 96, 165

Ivanov, B., A., Neukum, G., Bottke jr., W., F., Hartmann, W., F., 2001, Asteroids III

Ivanov, B., A., Neukum, G., Bottke jr., W., F., Hartmann, W., F., 2002, Icarus, 77, 203

Salamunicćar, G., Lončarić, S., Mazarico, E., 2012, Planetary and Space Science, 236, 60

Salamunicćar, G., Lončarić, S., 2012, IEEE Transactions on Geoscience and Remote Sensing, 2317, 48, 5

Salamunićcar G., Lončarić S., Vinković D., Vučina D., Gomerčić M., Pehnec I., Vojković M., Hercigonja T., 2012, Planetary and Space Science, 71, 106

Schwenzer S. P., et al., 2012, Earth and Planetary Science Letters, 335, 9

Skinner Jr., J., A., Hare, T., M., Tanaka, K., L., 2006, Lunar and Planetary Science XXXVII

Smith, D., E., Zuber, M., T., Herbert, W., Garvin J., B., 2001, Journal of Geophysical Research, 106

Stepinski, T., F., Urbach, E., R., 2007, 7^{th} International Conference on Mars

Stepinski, T., F., Mendenhall, M., P., Bue, B., D., 2009, Icarus, 77, 203

Stepinski, T., F., 2010, 41^{st} Lunar and Planetary Science Conference

Tanaka, K., 1986, Journal of Geophysical Research, 91

Treiman, A., "Maps of Mars", Lunar and Planetary Institute, 10 Jan. 2003. Web. 15 Oct. 2012. $http://www.lpi.usra.edu/science/treiman/greatdesert/workshop/marsmaps1/$